MODELLING, SIMULATION AND DYNAMICS OF A SYNCH-ROTOR AIRCRAFT

Giulia Bertolani, giulia.bertolani2@unibo.it, University of Bologna (Italy)

Emanuele Luigi de Angelis, emanuele.deangelis4@unibo.it, University of Bologna (Italy)

Fabrizio Giulietti, fabrizio.giuliett@unibo.it, University of Bologna (Italy)

Gianluca Rossetti, gianluca.rossetti3@unibo.it, University of Bologna (Italy)

Abstract

This paper presents a detailed modelling, control system design, and numerical simulation of a rotary wing aircraft with two synchronised rotors. Following the derivation of the complete non-linear 6 DoF equations, a nested loop control architecture made of attitude stabilisation and trajectory tracking is designed after a linearisation process. Numerical simulation and performance analysis are carried out. Results concerning hovering and forward flight, relevant from the perspective of practical applications are presented and discussed. The synch-rotor configuration appears suitable and effective for application where Unmanned Aerial Systems are foreseen such as environment monitoring, aerial photogrammetry, and load transportation.

NOMENCLATURE

a_0	Rotor coning angle (rad)
a_1	Longitudinal rotor tip path plane deflection angle in rotor-hub system (rad)
A_{1c}	Lateral cyclic pitch measured from hub plane in Wind-Hub axes system(rad)
A_{1s}	Lateral cyclic pitch measured from hub plane in Hub-Body axes system(rad)
b_1	Lateral rotor tip path plane deflection angle in rotor-hub system (rad)
B_{1c}	Longitudinal cyclic pitch measured from hub plane in Wind-Hub axes system(rad)
B_{1s}	Longitudinal cyclic pitch measured from hub plane in Hub-Body axes system(rad)
$\widetilde{D}$	Damping matrix
e	Flapping hinge offset (m)
$\tilde{f}$	Forcing function
$\widetilde{K}$	Stiffness matrix
K_1	Pitch-flap coupling ratio
K_I	Integral gain
K_P	Proportional gain
K_D	Derivative gain
M_β	Blade weight moment about the flapping hinge (kg/m^2)
R	Rotor radius (m)
U_T	
U_P	
$\mathbf{I} = diag(I_x, I_y, I_z)$	Inertia tensor (kg/m^2)
$\boldsymbol{F}^{(.)} = [X \quad Y \quad Z]^T$	Forces vector (N)
$\boldsymbol{M}^{(.)} = [L \quad M \quad N]^T$	Moments vector (Nm)
$\boldsymbol{V}^{(.)} = [u \quad v \quad w]^T$	Linear velocity vector (m/s)
$\boldsymbol{\Omega}^{(.)} = [p \quad q \quad r]^T$	Angular velocity vector (rad/s)
β	Blade flapping (rad)
ε	Hinge offset ratio
μ	Advance ratio
ϕ, θ, ψ	Roll, pitch, yaw Euler angles (rad)
θ_0	Blade root collective pitch (rad)
Ω	Rotor angular velocity (rad/s)
	Subscripts
b	Body frame
cl	Clockwise
ccl	Counter-clockwise
e	Earth fixed NED frame
e	Equilibrium condition

Presented at 46th European Rotorcraft Forum, Moscow, Russia, 8-11 September, 2020

This work is licensed under the Creative Commons Attribution International License (CC BY). Copyright © 2020 by author(s).

fus	Fuselage
h	Hub-Body frame
$hor\ stab$	Horizontal stabilizer
LV	Local-Vertical frame
mr	Main rotor
$vert\ stab$	Vertical stabilizer
w	Wind-Hub frame
	Superscripts
a	Aerodynamical
e	External
g	Gravitational

1. INTRODUCTION

The use of Unmanned Aerial Systems (UAS) is increasingly growing in a number of application areas. This is particularly true for battery-powered rotary-wing platform because their small size, light weight and low cost, and hovering capability. In this scenario, helicopter configurations and related technologies are a sound reality either as research platforms or commercial products manufactured by several companies all over the world. Among much research dedicated to small-scale helicopter modeling and control, this paper presents the result of a research activity focused on the mathematical modelling of a synch-rotor aircraft (intermeshing rotors) and its performance and dynamic behavior analysis.

Since existing applications of this rotor configuration are related to the Kaman K-MAX®, Ref. [1] and other few small-scale platform projects Ref. [2], [3] , a suitable mathematical model for simulating purposes as well as a detailed performance analysis and dynamical behavior description are still missing. As a matter of fact, most of the current research focuses on performances analysis based on experimental validation rather than providing a generalized theoretical framework for addressing preliminary design, optimal sizing and control system design. Moreover, the few existing models obtained from Kaman K-MAX® (and other small unmanned platforms) by means of systems identification algorithms, they do not provide close analytical description of dynamics modes; thus, a description of the relationship between aircraft design and its dynamics features is also still missing.
Synch-rotor configuration is becoming attractive among rotary-wing unmanned platform. As a matter of fact, with respect to conventional single main rotor helicopter configuration, its load capacity, endurance and low noise, make such configuration suitable for Earth observation and monitoring, Search&Rescue, and load transportation tasks.

This paper presents a detailed dynamic modelling, simulation and preliminary control system of an unmanned synch-rotor platform. The design process of this configuration is a challenging task; on one side, the absence of a tail rotor drive to an exceptional high ratio of lift per horsepower and a very stable hovering performance, on the other side two overlapping rotors allows for a more compact design (with respect a single main rotor of the same area) while affecting the overall aerodynamic efficiency. This makes the detailed modelling a mandatory tool for optimal sizing, especially in the early phases of aircraft design.

The proposed mathematical model, implemented in Matlab®/Simulink® environment, is made of the complete non-linear equations of motion and it includes the modelling of forces and moments acting on the vehicle. Aircraft dynamics and kinematics is represented by means of 16 DoF equations of motion: six equations rigid-body dynamics, six for attitude and position kinematics, three for rotor flapping dynamics, and one for rotor motion. Thus, a linear model is obtained by means of a linearization procedure related to a defined flight condition, and a set of controllers allowing for attitude stabilisation and trajectory tracking has been designed.

The rest of the paper is organised as follows: in Section 2 the full mathematical model and control system design is presented, whereas numerical results are included in Section 3. A Section of concluding remarks ends the paper.

2. MATHEMATICAL MODELLING

2.1. Aircraft dynamic

The proposed mathematical framework consists of the complete non-linear equations of motions and it includes the modelling of forces and moments acting on the vehicle.

2.1.1. Reference frames and coordinate transformation

Six orthogonal reference frames are introduced: Hub-Wind; Hub-Body, Body, Aircraft and Local Wind. In particular, the term "Hub" means that the origin of the coordinate system is at the hub centre. The terms "Wind" and "Body" indicate where the three axes point.

1. An Earth-fixed North–East-Down frame, $\mathbb{F}_E = \{O;\ \boldsymbol{x}_E, \boldsymbol{y}_E, \boldsymbol{z}_E\}$. This frame is inertial under the assumption of flat and non-rotating Earth.

Presented at 46th European Rotorcraft Forum, Moscow, Russia, 8-11 September, 2020
This work is licensed under the Creative Commons Attribution International License (CC BY). Copyright © 2020 by author(s).

2. Hub Wind Frame $\mathbb{F}_{hw} = \{H;\ \boldsymbol{x}_{hw}, \boldsymbol{y}_{hw}, \boldsymbol{z}_{hw}\}$. This frame is used in calculation of rotor forces and moments. Its origin is the rotor hub. $\mathbf{z}_{hw}$ axis is aligned with the rotor shaft, pointing upward. $\mathbf{x}_{hw}$ axis (horizontal) is aligned with the component of relative wind normal to the shaft axis. $\mathbf{y}_{hw}$ axis completes the right-handed orthogonal set.
3. Hub Body Frame $\mathbb{F}_{hb} = \{H;\ \boldsymbol{x}_{hb}, \boldsymbol{y}_{hb}, \boldsymbol{z}_{hb}\}$. $\mathbf{z}_{hb}$ axis is aligned with rotor shaft, pointing upward. This system coincides with the hub-wind system when the sideslip β_w is zero.
4. Body Fixed Frame $\mathbb{F}_b = \{P;\ \boldsymbol{x}_b, \boldsymbol{y}_b, \boldsymbol{z}_b\}$. Origin is located at the centre of gravity of the rotorcraft. $\mathbf{x}_b$ axis points in forward direction, it's aligned with the longitudinal axis of the vehicle; $\mathbf{z}_b$ axis points downward and $\mathbf{y}_b$ axis completes the right-hand system. All forces and moments used in the body equations of motion are expressed relative to this system.
5. Aircraft Frame $\mathbb{F}_a = \{A;\ \boldsymbol{x}_a, \boldsymbol{y}_a, \boldsymbol{z}_a\}$. The origin is typically located ahead and below the rotorcraft at some arbitrary point within the plane of symmetry. The reference axes are parallel to the Body axes, but $\mathbf{z}_a$ axis, called Waterline, points upward; $\mathbf{x}_a$ axis, named Stationline, points from bow to stern; $\mathbf{y}_a$ axis, Buttline, is positive to the pilot's right. All forces and moments and centre of gravity are located with these reference axes.
6. A set of Local Wind Frame $\mathbb{F}_{jw} = \{R_j;\ \boldsymbol{x}_{jw}, \boldsymbol{y}_{jw}, \boldsymbol{z}_{jw}\}$. These axes are used to calculate lift and drag forces on empennage and on the fuselage. For each surface, the origin is at the quarter point of the mean aerodynamic chord and the lift is normal to the relative wind and to a spanwise line passing through the quarter chord point.
7. Local Vertical Frame $\mathbb{F}_{LV} = \{P;\ \boldsymbol{x}_{LV}, \boldsymbol{y}_{LV}, \boldsymbol{z}_{LV}\}$. Origin is at the centre of gravity and axes are parallel to the inertial frame.

Rotor flapping dynamics assessment and rotor forces and moments calculation require linear and angular velocity vectors and acceleration vector as expressed in the Hub-Body system and the angle of sideslip at the hub. The cyclic pitch is also requested in Hub-Wind system.
In this respect, the velocity vector at the hub is written as follows:

$$\mathbf{V}_h = \Pi_{hb}(\mathbf{V} + \begin{bmatrix} l_{mr} \\ y_{mr} \\ h_{mr} \end{bmatrix} \times \boldsymbol{\Omega}) \tag{1}$$

whereas angular velocity and acceleration are given by:

$$\boldsymbol{\Omega}_h = \Pi_{hb}\boldsymbol{\Omega}_b \tag{2}$$

$$\dot{\boldsymbol{\Omega}}_h = \Pi_{hb}\dot{\boldsymbol{\Omega}}_b \tag{3}$$

where Π_{hb} is the rotational matrix from Body to Hub-Body system. Since rotors shafts are tilted in YZ plane in opposite directions with the same tilt angle i_s, Π_{hb} are different. For the right rotor one has:

$$\Pi_{hb} = \begin{bmatrix} 1 & 0 & 0 \\ 0 & \cos i_s & \sin i_s \\ 0 & -\sin i_s & \cos i_s \end{bmatrix} \tag{4}$$

whereas for the left one:

$$\Pi_{hb} = \begin{bmatrix} 1 & 0 & 0 \\ 0 & \cos i_s & -\sin i_s \\ 0 & \sin i_s & \cos i_s \end{bmatrix} \tag{5}$$

Calculated Wind-Hub system components are then rotated in order to be implemented into the 6-DOF equations of motion:

$$\begin{bmatrix} (\quad)_x \\ (\quad)_y \end{bmatrix}_{wh} = \begin{bmatrix} \cos\beta_w & \sin\beta_w \\ -\sin\beta_w & \cos\beta_w \end{bmatrix} \begin{bmatrix} (\quad)_x \\ (\quad)_y \end{bmatrix}_{hb} \tag{6}$$

where

$$\beta_w = \sin^{-1}\frac{v_h}{(v_h^2 + u_h^2)^{1/2}} \tag{7}$$

is the sideslip angle. The transformation matrix Π_{LVe} from Earth-fixed NED frame to Local Vertical frame is:

$$\Pi_{LVe} = \begin{bmatrix} \cos\psi & \sin\psi & 0 \\ -\sin\psi & \cos\psi & 0 \\ 0 & 0 & 1 \end{bmatrix} \tag{8}$$

and it is applied to forward and right velocities before entering the speed control system described below.

2.1.2. Equations of motions

Rotorcraft dynamics is described by Newton-Euler equations of motion projected in $\mathbb{F}_b$. Namely:

$$\dot{\mathbf{V}} = -\boldsymbol{\Omega} \times \mathbf{V} + \mathbf{F}^{(e)}/m \tag{9}$$

$$\dot{\boldsymbol{\Omega}} = \mathbf{I}^{-1}[-\boldsymbol{\Omega} \times (\mathbf{I}\boldsymbol{\Omega}) + \mathbf{M}^{(e)}] \tag{10}$$

where mass and mass distribution are assumed to be constant.
Rotorcraft attitude kinematics is given by:

$$\dot{\alpha} = \begin{bmatrix} 1 & \sin\phi\tan\theta & cos\phi\tan\theta \\ 0 & \cos\phi & -\sin\phi \\ 0 & \sin\phi/\cos\theta & \cos\phi/\cos\theta \end{bmatrix} \boldsymbol{\Omega} \tag{11}$$

Presented at 46th European Rotorcraft Forum, Moscow, Russia, 8-11 September, 2020
This work is licensed under the Creative Commons Attribution International License (CC BY). Copyright © 2020 by author(s).

$$\frac{d}{dt}\begin{bmatrix} x \\ y \\ z \end{bmatrix} = R_b^{hb}\begin{bmatrix} u \\ v \\ w \end{bmatrix} \tag{12}$$

provided

$$R_b^{hb} = \begin{bmatrix} c\theta c\psi & s\phi s\theta c\psi - c\phi s\psi & c\phi s\theta c\psi + s\phi s\psi \\ c\theta s\psi & s\phi s\theta s\psi + c\phi c\psi & c\phi s\theta s\psi - s\phi c\psi \\ -s\theta & s\phi c\theta & c\phi c\theta \end{bmatrix} \tag{13}$$

2.1.3. Forces and moments

The external forces are made of aerodynamic forces $\boldsymbol{F}^{(a)}$ and gravity forces $\boldsymbol{F}^{(g)}$ contributions, whereas total moments include aerodynamic moments $\boldsymbol{M}^{(a)}$.
Gravity forces are expressed in the following way:

$$\mathbf{F}^{(g)} = \Pi_{be}\begin{bmatrix} 0 \\ 0 \\ mg \end{bmatrix} = \begin{bmatrix} -mg\sin\theta \\ mg\sin\phi\cos\theta \\ mg\cos\phi\cos\theta \end{bmatrix} \tag{14}$$

Aerodynamic effects are introduced for all rotorcraft components and summed:

$$\mathbf{F}^{(a)} = \mathbf{F}^{(rot.)} + \mathbf{F}^{(fus.)} + \mathbf{F}^{(vert.stab.)} + \mathbf{F}^{(horiz.stab.)} \tag{15}$$

$$\mathbf{M}^{(a)} = \mathbf{M}^{(rot.)} + \mathbf{M}^{(fus.)} + \mathbf{M}^{(vert.stab.)} + \mathbf{M}^{(horiz.stab.)} \tag{16}$$

Main rotors model

Of the many components that form a rotorcraft, rotors are the main source of generation forces and moments. The intermeshing rotors model is made of two single-main rotor equations corrected by interference effects. Since rotors are counter-rotating and rotor equations are written for a counter-clockwise rotor, instead of re-derive equations for the opposite rotational direction, symmetrical coordinate systems are used Ref [4].

Equations for a single counter-clockwise rotor are derived. Blades are assumed rigid with integral form dependent on control actions, vehicle cinematics and flapping equations. Rotor is assumed as a teetering one. Flapping dynamics is approximated using a tip-path plane representation Ref [5]. The following assumptions are introduced:

1. Rotor blade is rigid in bending and torsion;
2. Linear blade twist;
3. Flapping and inflow angles are assumed small, the analysis is based on a simple strip theory;
4. Only effects due to angular acceleration $\dot{p}$ and $\dot{q}$, angular velocity p, q and the normal acceleration of the aircraft motion are considered to calculate blade flapping;
5. Compressibility and stall effects are not considered;
6. Reversed flow region is not considered;
7. The inflow is assumed to be uniform and no inflow dynamics are used;
8. The tip loss factor is assumed to be 1;
9. Blade flapping is approximated by the first harmonic terms with time-varying coefficients, that is:

$$\beta(t) = a_0(t) - a_1(t)\cos\psi - b_1(t)\sin\psi \tag{17}$$

The analytical tip-path plane dynamic equations are:

$$\ddot{\bar{\mathbf{a}}} + \tilde{D}\dot{\bar{\mathbf{a}}} + \tilde{K}\bar{\mathbf{a}} = \tilde{\bar{f}} \tag{18}$$

where $\boldsymbol{a} = (a_0 \quad a_1 \quad b_1)^T$ and expressions for $\widetilde{D}$, $\tilde{K}$, $\tilde{f}$ terms are reported in Appendix A for the sake of clarity. According to blade flapping approximation in Eq. (17), a_0 is treated as a preset constant and coefficients $a_1(t)$ and $b_1(t)$ can be solved for by setting $\varepsilon = \dot{a}_0 = \ddot{a}_0 = 0$ in Eq. (18).
Given the above assumptions, in conjunction with the development of tip-path plane dynamic equations, in forces and moments equations momentum theory is utilized and blade forces are analytically integrated over the radius. Contributions functions of the azimuth of each blade are summed. Outcomes of Ref [6] show that results are valid up to an advance ratio of 0.3. Equations are first obtained in the Wind-Hub coordinate system and then transformed into Body system. Forces and moments expressions, with the harmonic terms dropped that correspond to the number of rotor blades are given below. In order to illustrate the procedure, only the development of the thrust is shown. The shear force for a single i^{th} blade at azimuth ψ_i is given by:

$$\begin{aligned} S(\psi_i) =& F_a - \ddot{\beta}M_\beta - mq + m(\dot{w} - uq + pv) \\ &+ [2p\Omega(\frac{M_\beta}{g} + em) + \frac{M_\beta}{g}\dot{q}]\cos\psi_i' \\ &+ [-2q\Omega(\frac{M_\beta}{g} + em) + \frac{M_\beta}{g}\dot{p}]\sin\psi_i' \end{aligned} \tag{19}$$

where the aerodynamic force, is given by:

$$F_a = \int_0^{R-e} \frac{\rho}{2}(\Omega R)^2 ac(\bar{U}_T^2\theta + \bar{U}_T\bar{U}_P)\,dr' \tag{20}$$

Let's substitute the following equations in equation (20):

$$\bar{U}_T = \frac{U_T}{\Omega R} = \epsilon(1-\cos\beta) + \mu\sin\psi + x\cos\beta \tag{21}$$

$$\begin{aligned} \bar{U}_P = \frac{U_P}{\Omega R} =& \lambda\cos\beta - \mu\sin\beta\cos\psi - \frac{\dot{\beta}}{\Omega}(x-\epsilon) \\ &+ x[(\frac{p}{\Omega}\cos\beta_w + \frac{q}{\Omega}\sin\beta_w)\sin\psi \\ &+ (-\frac{p}{\Omega}\sin\beta_w + \frac{q}{\Omega}\cos\beta_w)\cos\psi] \end{aligned} \tag{22}$$

$$\theta = \theta_0 - A_{1c}\cos\psi - B_{1c}\sin\psi + x\theta_t - K_1\beta \tag{23}$$

Presented at 46th European Rotorcraft Forum, Moscow, Russia, 8-11 September, 2020
This work is licensed under the Creative Commons Attribution International License (CC BY). Copyright © 2020 by author(s).

So $\boldsymbol{F}^a$ results:

$$\begin{aligned}F_a =&\frac{\rho}{2}(\Omega R)^2 acR\{[\frac{1}{3}+(1-\epsilon)(1+\epsilon+\\&\mu\sin\psi)\mu\sin\psi](\theta_0-A_{1c}\cos\psi-B_{1c}\sin\psi)\\&+[\frac{1}{4}+(\frac{2}{3}+\frac{1}{2}1-\epsilon^2\mu\sin\psi)\mu\sin\psi]\theta_t\\&+[\frac{1}{2}(1-\epsilon^2)+(1-\epsilon)\mu\sin\psi]\lambda\\&-\{[\frac{1}{3}+(1-\epsilon)(1+\epsilon+\mu\sin\psi)\mu\sin\psi]K_1\\&+[\frac{1}{2}(1-\epsilon^2)+(1-\epsilon)\mu\sin\psi]\mu\cos\psi\}\beta\\&-\frac{1}{\Omega}[\frac{1}{3}-\frac{\epsilon}{2}+\frac{\mu}{2}(1-\epsilon)^2\sin\psi]\dot{\beta}\\&+[\frac{1}{3}+\frac{\mu}{2}(1-\epsilon^2)\sin\psi]\\&[(\frac{p}{\Omega}\cos\beta_w+\frac{q}{\Omega}\sin\beta_w)\sin\psi\\&+(-\frac{p}{\Omega}\sin\beta_w+\frac{q}{\Omega}\cos\beta_w)\cos\psi]\}\end{aligned} \tag{24}$$

Flapping dynamics is approximated as in Eq. (17) and:

$$\dot{\beta}=\dot{a}_0-(\dot{a}_1+b_1\Omega)\cos\psi-(\dot{b}_1-a_1\Omega)\sin\psi \tag{25}$$

$$\begin{aligned}\dot{\beta}=&\dot{a}_0-(\dot{a}_1+b_1\Omega)\cos\psi\\&-(\dot{b}_1-a_1\Omega)\sin\psi\end{aligned} \tag{26}$$

noting that:

$$\begin{aligned}\sum_{i=1}^{N}\cos\psi_i=\sum_{i=1}^{N}\cos\psi_i'=0\\\sum_{i=1}^{N}\sin\psi_i=\sum_{i=1}^{N}\sin\psi_i'=0\end{aligned} \tag{27}$$

The thrust is then given by:

$$\begin{aligned}T=&\sum_{i=1}^{N}F_a(\psi_i)-N[\ddot{a}_0M_\beta+mg\\&-m(\dot{w}-uq+pv)]\end{aligned} \tag{28}$$

For $N=2$, dropping the high harmonic contributions, thrust modulus is expressed as:

$$\begin{aligned}T=&\frac{N}{2}\rho acR(\Omega R)^2\{\frac{1}{2}(1-\epsilon^2)\lambda+\\&[\frac{1}{3}+\frac{\mu^2}{2}(1-\epsilon)]\theta_0\\&+[\frac{1}{4}+\frac{\mu^2}{4}(1-\epsilon^2)]\theta_t\\&-\frac{\mu}{2}(1-\epsilon^2)(B_{1c}-K_1b_1)-a_=\\&[\frac{1}{3}+\frac{\mu^2}{2}(1-\epsilon)]K_1+a_1[\frac{\mu}{2}\epsilon(1-\epsilon)]\\&-\frac{\dot{a}_0}{\Omega}(\frac{1}{3}-\frac{\epsilon}{2})+\frac{\dot{b}_1}{\Omega}[\frac{\mu}{4}(1-\epsilon)^2]\\&+\frac{\mu}{4}(1-\epsilon^2)(\frac{p}{\Omega}\cos\beta_w+\frac{q}{\Omega}\sin\beta_w)\}\\&-N\ddot{a}_0M_\beta\end{aligned} \tag{29}$$

The same procedure is applied for the other equations and results are reported in Appendix C of Ref [5].

Solution for a two-bladed teetering rotor $\varepsilon=\dot{a}_0=\ddot{a}_0=0$ is set in the forces and moments equations. The rotor inflow ratio is required in the computation of thrust. It is given in an implicit form in Eq. (30) and it's solved in the program through a Newton-Raphson iterative method.

$$\lambda=\frac{w_H}{\Omega R}-\frac{C_T}{2(\mu^2+\lambda^2)^{1/2}} \tag{30}$$

The expression of rotor-induced velocity at the disk, required in the calculation is:

$$v_i=(\frac{w_H}{\Omega R})\Omega R \tag{31}$$

Derivation of tip-path plane dynamic equation is detailed in Ref [7].

Obtained equations are now applied to counter-clockwise rotor by using the left-hand coordinate system and using a direction indicator χ in lateral equations, which value is equal to 1 when rotor is counter-clockwise; -1 otherwise. Resulting equations are given as follows:

$$\begin{aligned}\boldsymbol{V}_{cl}&=\Pi_1\boldsymbol{V}_{ccl}\\\boldsymbol{\Omega}_{cl}&=\Pi_2\boldsymbol{\Omega}_{ccl}\\\boldsymbol{F}_{cl}&=\Pi_1\boldsymbol{F}_{ccl}\\\boldsymbol{M}_{cl}&=\Pi_2\boldsymbol{M}_{ccl}\\\boldsymbol{U}_{cl}&=\Pi_1\boldsymbol{U}_{ccl}\end{aligned} \tag{32}$$

provided $\Pi_1=\begin{bmatrix}1&0&0\\0&\chi&0\\0&0&1\end{bmatrix}$, $\Pi_2=\begin{bmatrix}\chi&0&0\\0&1&0\\0&0&\chi\end{bmatrix}$ and

$\boldsymbol{U}=[\theta_0\quad A_{1s}\quad B_{1s}]$.

Fuselage model

The fuselage aerodynamic model provides forces and moments as a function of angle of attack and sideslip angle along the flight envelope. Effects are

Presented at 46th European Rotorcraft Forum, Moscow, Russia, 8-11 September, 2020

This work is licensed under the Creative Commons Attribution International License (CC BY). Copyright © 2020 by author(s).

accounted into performance and stability analysis for forward speeds. Continuity in numerical estimation is mandatory in order to prevent unrealistic linear or angular accelerations in response to small changes in attitude. In the case of extreme attitudes, accuracy of the model becomes less relevant because at high speeds, fuselage forces and moments are very small if compared to those generated by rotors.
A widely used technique provides a continuous model by fitting forces and moments variations through data points obtained by wind-tunnel tests at specific widely separated angles of attack and sideslip angles. However, these data are often unavailable. In this model, continuity is provided by a linear interpolation for forces and moments on angles range not covered. Data for lower angles range are obtained by test or from estimates on similar fuselage. Data for higher range are based on estimated magnitude and location of the drag force vector when the fuselage is in a 90° cross flow. Details on the procedure and forces and moments equations are available in Ref [5].

Vertical and horizontal stabilizer model

Vertical fin and horizontal tail are considered as lift and drag producers and are approximated for all angles of attack and sideslip. Principal assumptions include:

1. Surfaces are modelled with symmetrical profiles;
2. An elliptical distribution with uniform downwash is considered;
3. Forces are applied at the quarter chord of each surface;
4. Maximum lift coefficient is specified;
5. Profile drag coefficient varies with angle of attack;
6. The induced drag coefficient at the square of the calculated lift coefficient.

Equations are given in detail in Ref [5].

2.1.4. Rotors interference

Interference effects are included and modelled considering the overlapping between the two rotors. These effects are consistent to those in Ref [8], but, since rotors are not coaxial as in Leishman paper, the overlapping area is calculated and a rotor-interference induced power factor, a scaling factor, *k* is introduced. The value of this factor is calculated from Leishman's value of k_{int} multiplied by a scaling factor representing the overlapping area between the rotors.
This area is calculated projecting the radius of a single tilted rotor from XY Hub-Body plane to the un-tilted *XZ* Body plane and considering the length of overlapping distance. The area is geometrically estimated, whereas seen from the top it appears as an intersection of two circular sectors. Then equivalent radius is estimated and the ratio between the areas is found. Finally, the interference induced power factor results to be scaled by this ratio and it's used in power calculation in the same way as in Ref [8]. Reference case 2 (Corotation in the same plane at balanced torque) for coaxial rotors system of those discussed by Leishman in its paper is chosen for this analysis. Equations for scaling factor are as follows:

(33) $$A_{overlapping} = 2 * A_{circ\ sect} - A_r$$

where $A_{circ\ sect} = \frac{R_{projected}{}^2 * \alpha}{2}$, $R_{projected} = R\cos i_s$, $\alpha = 2\cos^{-1}(\frac{d_{hub}}{R_{projected}})$, $A_r = d_{hub} * R_{projected} * \sin\frac{\alpha}{2}$ and d_{hub} is the distance between the two rotors hub.

2.1.5. Linearized equations of motion

Let $\boldsymbol{f}(\dot{\boldsymbol{X}}, \boldsymbol{X}, \boldsymbol{U}, t) = 0$ represent the non-linear model described by the equations (8), (9), (10), (11) where $\boldsymbol{X} = \{u, w, q, \theta, v, p, \phi, r, \psi\}$ is the state vector and $\boldsymbol{U} = \{A_{1s},\ \theta_0, B_{1s+}, B_{1s-}\}$ is the control vector. With small perturbation theory, it can be assumed that during disturbed motion, the vehicle behaviour can be described as a perturbation from the equilibrium condition, written in the form:

(34) $$\boldsymbol{X} = \boldsymbol{X}_e + \delta\boldsymbol{X}$$

where $\delta\boldsymbol{X}$ represent the perturbated state. Linearized equations in state-space form

(35) $$\dot{\boldsymbol{X}} = \boldsymbol{A}\boldsymbol{X} + \boldsymbol{B}\boldsymbol{U}$$

are obtained numerically perturbating the system. This methodology is the most complete and accurate to evaluate dynamics, since analytical expressions for natural modes are not involved. Finite different method has been applied directly on simulation software Ref. [9].

2.2. Control system

Control system is based on Proportional-Integral-Derivative (PID) technique. It presents a cascade structure. This architecture is usually made by a primary controller and by primary dynamics that are the parts of the outer loop. A secondary controller is designed as part of the outer loop. Set-points for the inner loop are calculated by the outer one. Autopilots are designed under the assumption to that the inner loop presents faster dynamics than the outer one. In general, non-linear features of the plant are handled by the inner loop. Ref [10].

Inner loop controllers

Controllers of the inner loop are the attitude, the yaw and the altitude hold controller.

Presented at 46th European Rotorcraft Forum, Moscow, Russia, 8-11 September, 2020
This work is licensed under the Creative Commons Attribution International License (CC BY). Copyright © 2020 by author(s).

The attitude controller is based on a pitch/roll damper. Figure 1 show the design in detail.

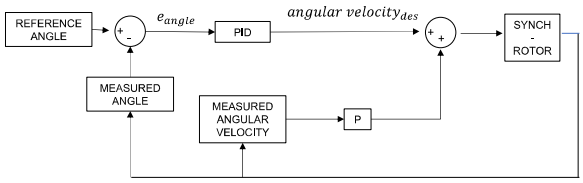

Figure 1: Attitude controller architecture

By defining the error signals as follows:

(36) $$e_x = x_{des} - x$$

where x represents the variable to be controlled, the attitude controller output can be resumed as:

(37) $$\begin{cases} A_{1s} = K_{Pp}p + p_{des} \\ B_{1pi} = K_{Pq}q + q_{des} \\ p_{des} = K_{P\phi}e_\phi - K_{D\phi}\dot{e}_\phi + K_{I\phi}\int_0^t e_\phi dt \\ q_{des} = K_{P\theta}e_\theta - K_{D\theta}\dot{e}_\theta + K_{I\theta}\int_0^t e_\theta dt \end{cases}$$

The yaw controller presents the same scheme of attitude controller. Its output is:

(38) $$\begin{cases} B_{1yaw} = K_{Pr}r + r_{des} \\ r_{des} = K_{P\psi}e_\psi - K_{D\psi}\dot{e}_\psi + K_{I\psi}\int_0^t e_\psi dt \end{cases}$$

Outputs B_{1pi} and B_{1yaw} are mixed to get commands values B_{1s+} and B_{1s-} as follows:

(39) $$\begin{aligned} B_{1s+} &= B_{1pit} + B_{1yaw} \\ B_{1s-} &= B_{1pi} - B_{1yaw} \end{aligned}$$

The altitude-hold controller is made of PID acting on reference altitude. Control architecture is depicted in Figure 2, and the output equation is given by:

(40) $$\theta_0 = K_{Ph}e_h - K_{Dh}\dot{e}_h + K_{Ih}\int_0^t e_h dt$$

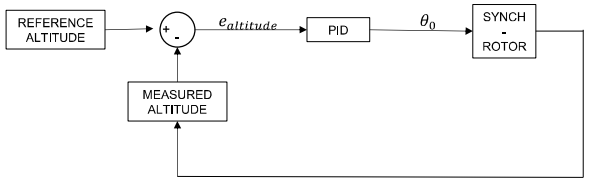

Figure 2: Altitude-hold controller architecture

Outer loop controllers

The outer loop controller is part of the main cascade control scheme and it is designed as a feedback PI controller fed by forward/right velocity references u_{des}, v_{des} and provides desired pitch/roll angles θ_{des}, ϕ_{des} to the inner control loop. Velocities are converted from Earth-fixed NED frame to Local Vertical one. Errors are calculated as in Eq. (36), controller scheme is shown in Figure 3. and resultant equations are:

(41) $$\begin{cases} \theta_{des} = K_{Pu}e_u + K_{I\theta}\int_0^t e_\theta dt \\ \phi_{des} = K_{P\phi}e_\phi + K_{I\phi}\int_0^t e_\phi dt \end{cases}$$

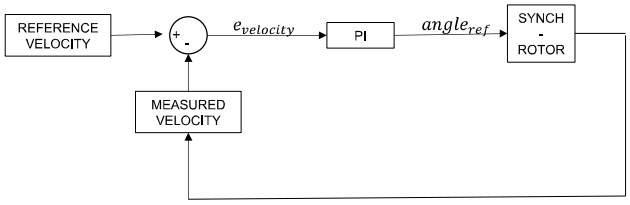

Figure 3: Velocity controller architecture

3. NUMERICAL SIMULATION

The presented model has been implemented in a soft-real time hardware in Matlab®/Simulink® environment and numerical simulation have been conducted. Results for controllers' attitude stabilisation and velocity tracking are first presented, then results of performance analysis are reported. Different flight conditions have been simulated.

Figure 4 shows the response of damper controllers to an initial perturbation of angular velocities in time. In order to test damper controllers, roll, pitch and yaw rates have been set as initial conditions different from zero $(0.2\ rad/s)$. The dynamic model uses a sample rate of $t = 0.01\ s$ and the simulation is $10\ s$ long.

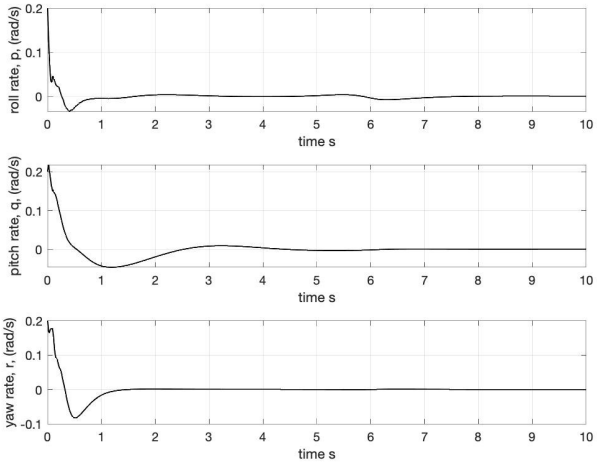

Figure 4: roll,pitch and yaw rate vs time.

Presented at 46th European Rotorcraft Forum, Moscow, Russia, 8-11 September, 2020
This work is licensed under the Creative Commons Attribution International License (CC BY). Copyright © 2020 by author(s).

Figure 5 shows the response of attitude controllers to desired roll, pitch and yaw angles in time. Simulations setting are the same of previous case, except for initial conditions, that are all equal to zero and the system is required to achieve desired angles values, fixed to $\mp 0.1\ rad$.

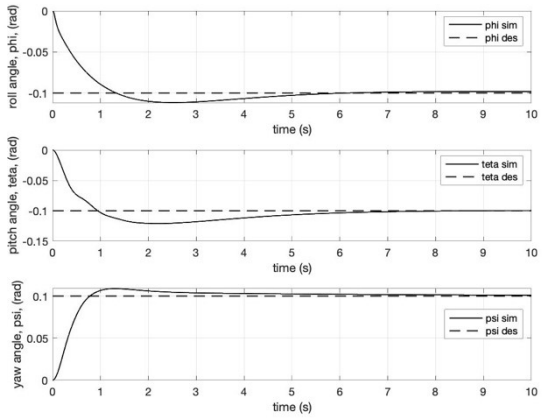

Figure 5: Roll, pitch and yaw angles vs time

Figure 6 shows the response of altitude-hold controller to a desired value in time. Again, hovering condition has been tested with sample rate of $t = 0.01\ s$; simulation time is $60\ s$, starting value for altitude is set to $100\ m$ and desired one is $150\ m$.

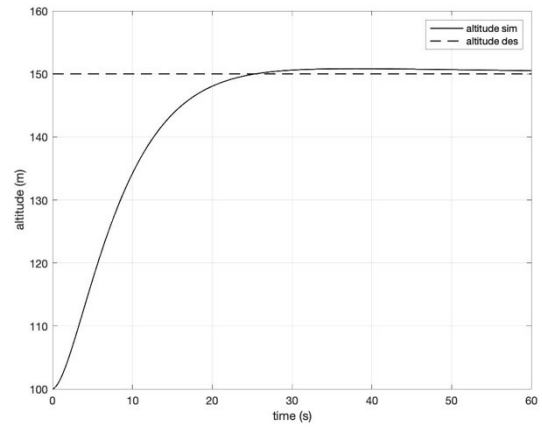

Figure 6: Simulated and desired altitude vs time

Illustrated results indicates the capability of the inner loop controller to stabilize the system to desired conditions.

Figure 7 shows the response of speed controller to a desired forward velocity in time. Forward flight has been tested this time to evaluate controller performance. Sample rate is the same of previous cases, simulation time is $20\ s$. The synch-rotor initial velocity is set to $0.5\ m/s$ in order to avoid singularities; desired forward flight is $50\ km/h$. Again, results suggest the ability of the speed controller to track a desired forward velocity.

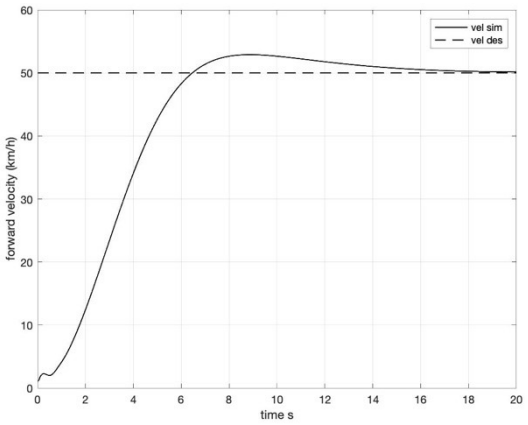

Figure 7: Forward velocity vs time

Performance analysis results are shown in Figure 8. Synch-rotor required power along the flight envelope is compared to the two isolated main-rotor configuration.

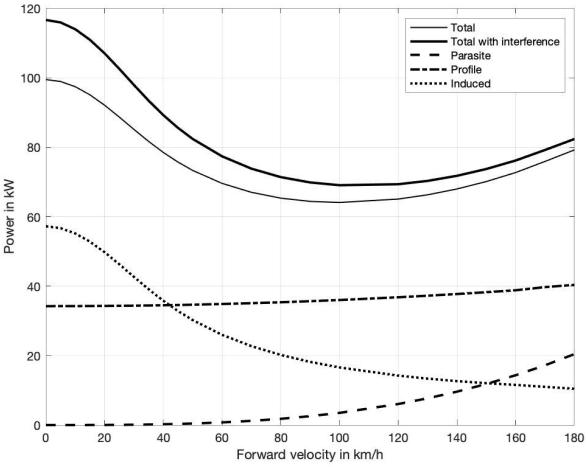

Figure 8: Power synch-rotor power required

As expected, total power required considering interference effects is higher and presents and decreases with increasing forward velocity.

4. CONCLUSIONS

This paper presented a detailed mathematical model of a synch-rotor aircraft and a preliminary control system design and performance assessment. The full nonlinear model has been linearised about the hovering and forward flight conditions, and stability derivatives are obtained addressing the relationship between dynamic behaviour and aircraft design.

Presented at 46th European Rotorcraft Forum, Moscow, Russia, 8-11 September, 2020
This work is licensed under the Creative Commons Attribution International License (CC BY). Copyright © 2020 by author(s).

In the present work, medium complexity models were considered for rotors' force and moments as well as SISO (Single-Input Single-Output) approach for control system design. In future works, more complex models for flapping dynamics, inflow and fuselage will be introduced together with a multivariable approach for attitude stabilisation and trajectory tracking.

5. REFRENCES

[1] M. H. Mansur, M. B. Tischler, M. D. Bielefield, J. W. Bacon, K. K. Cheung, M. G. Berrios and K. E. Rothman, "Full Flight envelope ineer-loop control law development for the unmanned K-MAX," in *67th American Helicopter Society Annual Forum*, Virginia Beach, VA, May 3-5, 2011.

[2] A. Barth, C. Spieb, K. Kondak and M. Hajek, "Design, Analysis and Flight Testing of a High Altitude Synchropter UAV," in *AHS International 74th Annual Forum&Technology Display*, Phoenix, Arizona, USA, May 14-17, 2018.

[3] F. S. J. Wei, E. Moore and A. Gates, "An intermeshing rotor helicopter design and test," in *AIAA SciTech 2015*, Kissimmee, Florida, January 5-9, 2015.

[4] H. S. Choi, E. T. Kim, D. I. You and H. Shim, "Improvements in Small-scale Helicopter Rotor Modeling for the Real-time Simulation of Hovering Flight," *The Japan Society for Aeronautical and Space Science,* vol. 54, no. 185/186, pp. 229-237, 2011.

[5] P. D. Talbot, B. E. Tinling, W. A. Decker and R. T. N. Chen, "A mathematical model for a single main rotor helicopter for piloted simulation," Ames Reasearch Center, Moffett, Field, California, September 1982.

[6] E. Seckel and J. Curtiss, "Aerodynamic characteristics of helicopter rotors," Dept. of Aerospace and Mechanical Eng., Princeton University, 1962.

[7] R. T. N. Chen, "A simplified rotor system mathematical model for piloted flight dynamics simulation," Ames Reaserach Center, NASA, Moffett Field, California, May 1979.

[8] J. G. Leishman and M. Syal, "Figure of merit definition for coaxial rotors," *Journal of the American Helicopter Society,* vol. 53, no. 3, pp. 290-300, July 2008.

[9] G. D. Padfield, Helicopter Flight Dynamics, Blackwell Publishing, 1996.

[10] G. Rossetti, *Development of a flight control architecture for rotary-wing UAVs with model-based design approach,* 2017.

[11] B. Theys, G. Dimitridias, P. Hendrick and J. De Schutter, "Influence of propeller configuration on propulsiion system efficency of multi-rotor Unmanned Aerial Vehicles," in *International Conference of Unmanned Aircraft System (ICUAS)*, 2016.

Presented at 46th European Rotorcraft Forum, Moscow, Russia, 8-11 September, 2020

This work is licensed under the Creative Commons Attribution International License (CC BY). Copyright © 2020 by author(s).

APPENDIX A

Expressions for stiffness matrix $\tilde{K}$, damping matrix $\tilde{D}$ and forcing factor $\tilde{f}$:

$$\ddot{\underline{a}} + \tilde{D}\underline{\dot{a}} + \tilde{K}\underline{a} = \tilde{f}$$

$$\tilde{D} = \Omega \begin{bmatrix} \frac{\gamma}{2}\left(\frac{1}{4} - \frac{2}{3}\varepsilon + \frac{\varepsilon^2}{2}\right) & 0 & -\frac{\gamma\mu}{4}\left(\frac{1}{3} - \varepsilon + \varepsilon^2\right) \\ 0 & \frac{\gamma}{2}\left(\frac{1}{4} - \frac{2}{3}\varepsilon + \frac{\varepsilon^2}{2}\right) & 2 \\ -\frac{\gamma\mu}{2}\left(\frac{1}{3} - \varepsilon + \varepsilon^2\right) & -2 & \frac{\gamma}{2}\left(\frac{1}{4} - \frac{2}{3}\varepsilon + \frac{\varepsilon^2}{2}\right) \end{bmatrix}$$

$$\tilde{K} = \Omega^2 \begin{bmatrix} P^2 + \frac{\gamma K_1 \mu^2}{4}\left(\frac{1}{2} - \varepsilon + \frac{\varepsilon^2}{2}\right) & -\frac{\gamma\mu}{4}\left(\frac{\varepsilon}{2} - \varepsilon^2\right) & -\frac{\gamma K_1 \mu}{4}\left(\frac{2}{3} - \varepsilon\right) \\ -\frac{\gamma\mu}{2}\left(\frac{1}{3} - \frac{\varepsilon}{2}\right) & P^2 - 1 + \frac{\gamma K_1 \mu^2}{8}\left(\frac{1}{2} - \varepsilon + \frac{\varepsilon^2}{2}\right) & \frac{\gamma}{2}\left(\frac{1}{4} - \frac{2}{3}\varepsilon + \frac{\varepsilon^2}{2}\right) + \frac{\gamma\mu^2}{8}\left(\frac{1}{2} - \varepsilon + \frac{\varepsilon^2}{2}\right) \\ -\frac{\gamma K_1 \mu}{2}\left(\frac{2}{3} - \varepsilon\right) & -\frac{\gamma}{2}\left(\frac{1}{4} - \frac{2}{3}\varepsilon + \frac{\varepsilon^2}{2}\right) + \frac{\gamma\mu^2}{8}\left(\frac{1}{2} - \varepsilon + \frac{\varepsilon^2}{2}\right) & P^2 - 1 + \frac{3}{8}\gamma K_1 \mu^2\left(\frac{1}{2} - \varepsilon + \frac{\varepsilon^2}{2}\right) \end{bmatrix}$$

$$\tilde{f} = \Omega^2 \begin{bmatrix} -\frac{M_\beta}{I_\beta \Omega^2} + \frac{\gamma}{2}\left[\left(\frac{1}{4} - \frac{\varepsilon}{3}\right) + \frac{\mu^2}{2}\left(\frac{1}{2} - \varepsilon + \frac{\varepsilon^2}{2}\right)\right]\theta_0 - \frac{\gamma}{2}\left[\mu\left(\frac{1}{3} - \frac{\varepsilon}{2}\right)\right] B_{1c} + \frac{\gamma}{2}\left[\left(\frac{1}{5} - \frac{\varepsilon}{4}\right) + \frac{\mu^2}{2}\left(\frac{1}{3} - \frac{\varepsilon}{2}\right)\right]\theta_t + \frac{\gamma}{2}\left(\frac{1}{3} - \frac{\varepsilon}{2}\right)\lambda \\ \quad + \frac{\gamma}{8}\mu\left(\frac{2}{3} - \varepsilon\right)\left(\frac{P_H}{\Omega}\cos\beta_w + \frac{q_H}{\Omega}\sin\beta_w\right) \\ -2\left(1 + \frac{eM_\beta}{gI_\beta}\right)\left(\frac{P_H}{\Omega}\cos\beta_w + \frac{q_H}{\Omega}\sin\beta_w\right) + \left(\frac{\dot{P}_H}{\Omega^2}\sin\beta_w - \frac{\dot{q}_H}{\Omega^2}\cos\beta_w\right) + \frac{\gamma}{2}\left[\left(\frac{1}{4} - \frac{\varepsilon}{3}\right) + \frac{\mu^2}{4}\left(\frac{1}{2} - \varepsilon + \frac{\varepsilon^2}{2}\right)\right]A_{1c} \\ \quad + \frac{\gamma}{2}\left(\frac{1}{4} - \frac{\varepsilon}{3}\right)\left(\frac{P_H}{\Omega}\sin\beta_w - \frac{q_H}{\Omega}\cos\beta_w\right) \\ -2\left(1 + \frac{eM_\beta}{gI_\beta}\right)\left(\frac{P_H}{\Omega}\sin\beta_w - \frac{q_H}{\Omega}\cos\beta_w\right) - \left(\frac{\dot{P}_H}{\Omega^2}\cos\beta_w + \frac{\dot{q}_H}{\Omega^2}\sin\beta_w\right) - \frac{\gamma}{2}\mu\left(\frac{2}{3} - \varepsilon\right)\theta_0 - \frac{\gamma\mu}{2}\left(\frac{1}{2} - \frac{2\varepsilon}{3}\right)\theta_t \\ \quad + \frac{\gamma}{2}\left[\left(\frac{1}{4} - \frac{\varepsilon}{3}\right) + \frac{3\mu^2}{4}\left(\frac{1}{2} - \varepsilon + \frac{\varepsilon^2}{2}\right)\right]B_{1c} - \frac{\gamma\mu}{2}\left(\frac{1}{2} - \varepsilon + \frac{\varepsilon^2}{2}\right)\lambda - \frac{\gamma}{2}\left(\frac{1}{4} - \frac{\varepsilon}{3}\right)\left(\frac{P_H}{\Omega}\cos\beta_w + \frac{q_H}{\Omega}\sin\beta_w\right) \end{bmatrix}$$

Presented at 46th European Rotorcraft Forum, Moscow, Russia, 8-11 September, 2020

This work is licensed under the Creative Commons Attribution International License (CC BY). Copyright © 2020 by author(s).